Fast and Robust Point Containment Queries on Trimmed Surface

ANCHANG BAO, Tsinghua University, China ENYA SHEN, Tsinghua University, China and Haihe Lab of ITAI, China JIANMIN WANG, Tsinghua University, China

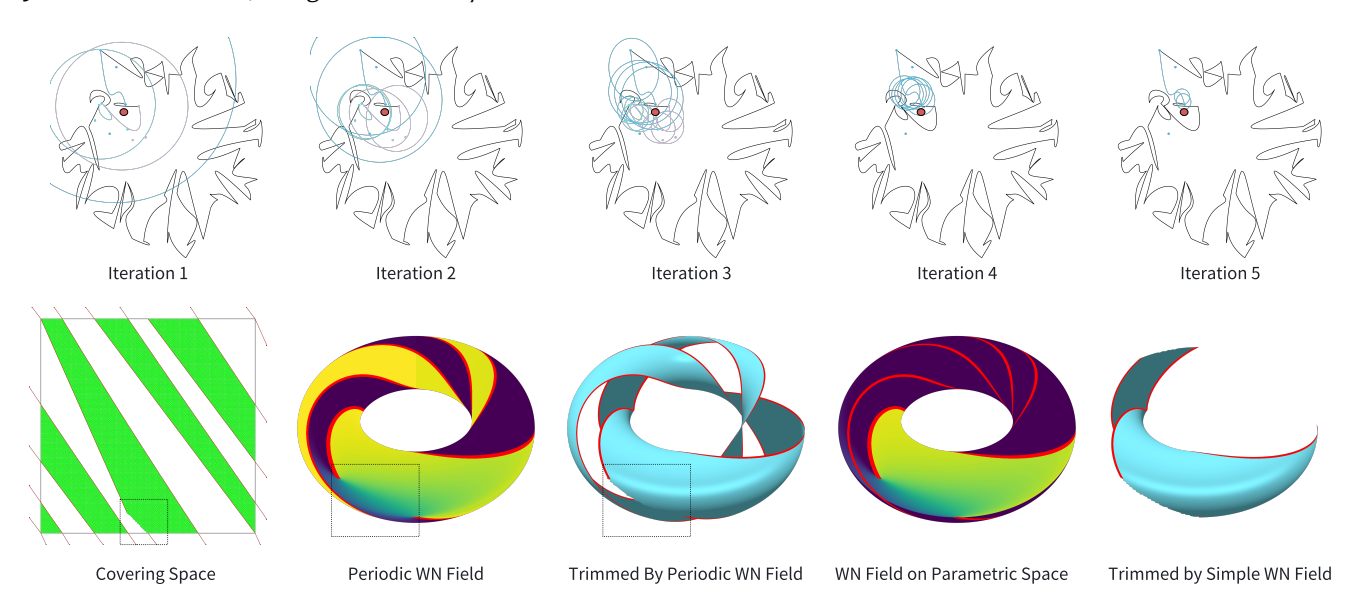


Fig. 1. We proposed an efficient winding number computation method for parametric curves and generalize to the periodic domain by lifting curves to the universal covering space. With this proposed method, we developed fast and robust point containment queries on trimmed surfaces. **First row**: Illustration of the winding number computation method described in section 4. The red point is the testing point and the colored curves are ellipses used in our algorithms. Different from the Spainhour et al. [2024], we utilize a more flexible ellipse bound, enabling linear time Bézier curves evaluation and O(1) inclusion test. **Second row**: By lifting curves to the universal covering space, we correctly compute the winding number on the periodic domain. With the proposed method, we can handle containment queries on the periodic trimmed surface robustly. Given open boundary curves, we present the winding number field calculated in covering space and parametric space respectively.

Point containment queries on trimmed surfaces are fundamental to CAD modeling, solid geometry processing, and surface tessellation. Existing approaches—such as ray casting and generalized winding numbers—often face limitations in robustness and computational efficiency.

We propose a fast and numerically stable method for performing containment queries on trimmed surfaces, including those with periodic parameterizations. Our approach introduces a recursive winding number computation scheme that replaces costly curve subdivision with an ellipse-based bound for Bézier segments, enabling linear-time evaluation. For periodic surfaces, we lift trimming curves to the universal covering space, allowing accurate

Authors' Contact Information: Anchang Bao, Tsinghua University, Beijing, China, baoanchang02@gmail.com; Enya Shen, Tsinghua University, Beijing, China and Haihe Lab of ITAI, Tianjin, China, shenenya@tsinghua.edu.cn; Jianmin Wang, Tsinghua University, Beijing, China, jimwang@tsinghua.edu.cn.

Permission to make digital or hard copies of all or part of this work for personal or classroom use is granted without fee provided that copies are not made or distributed for profit or commercial advantage and that copies bear this notice and the full citation on the first page. Copyrights for components of this work owned by others than the author(s) must be honored. Abstracting with credit is permitted. To copy otherwise, or republish, to post on servers or to redistribute to lists, requires prior specific permission and/or a fee. Request permissions from permissions@acm.org.

@ 2024 Copyright held by the owner/author(s). Publication rights licensed to ACM. ACM XXXX-XXXX/2024/10-ART

and consistent winding number computation even for non-contractible or discontinuous loops in parameter domain.

Experiments show that our method achieves substantial speedups over existing winding-number algorithms while maintaining high robustness in the presence of geometric noise, open boundaries, and periodic topologies. We further demonstrate its effectiveness in processing real B-Rep models and in robust tessellation of trimmed surfaces.

CCS Concepts: \bullet Computing methodologies \to Parametric curve and surface models.

Additional Key Words and Phrases: Trimmed surface, containment query, winding number

ACM Reference Format:

1 INTRODUCTION

Trimmed surfaces play a central role in free-form modeling and are commonly represented using Boundary Representation (B-Rep), the industry standard for free-form solids [Pratt et al. 2001]. Unlike ordinary spline patches, a trimmed surface is defined by an underlying geometric surface and a set of boundary curves that restrict its



Fig. 2. Containment queries on a trimmed torus. The opaque region represents the retained surface, while the translucent part is trimmed away. Points on the torus are randomly sampled; those inside the trimmed region are marked in red, and those outside are shown in green.

visible region. Processing boundary-represented solids lies at the core of free-form modeling, yet one key limitation of B-Rep is the absence of explicit containment relations between solids. As a result, containment tests become essential whenever inclusion relations are required. A fundamental instance of this task is determining whether a point on the underlying geometric surface lies within its trimmed region—known as a containment query on a trimmed surface. Figure 2 illustrates containment queries on a trimmed torus, a problem with broad applications in computer graphics, including CAD model processing, B-Rep ray tracing, and tessellation of trimmed surfaces.

Containment queries arise in a variety of CAD and modeling contexts. During Boolean operations between parametrically represented solids, numerous intersection edges are generated (Figure 3). Curve segments that lie on the underlying geometric surface but outside the trimmed region must be removed, which requires point–surface containment tests. Similarly, in ray-traced rendering of B-Rep models, rays may intersect the underlying surface at positions that must be verified as belonging to the trimmed region. Containment queries are also integral to trimmed-surface tessellation, where sample points in the parameter domain are classified as inside or outside the trimmed region before rendering.

In B-Rep, curves on surfaces are represented by a pair of mappings: a curve in physical space and its corresponding projection in the parameter domain, known as a **p-curve**. With p-curves, containment testing on non-periodic surfaces reduces to a 2D inside–outside test in the parameter domain. Ray-casting methods are commonly used for this purpose, but they are prone to corner cases and numerical instability. Winding-number–based methods, in contrast, are more robust but computationally expensive.

Containment queries on periodic domains are particularly challenging because the underlying topology alters how boundaries are represented. For example, when the geometric surface is cylindrical (Figure 4), the trimmed region is defined by separation loops. In such cases, the p-curves may not form closed loops in parameter domain, making standard trimming techniques such as ray casting or direct winding-number evaluation inadequate.

In this paper, we present a fast and robust framework for containment queries on trimmed surfaces. To ensure robustness against geometric and numerical errors, we adopt the winding number as the criterion for inside–outside classification. We introduce an efficient acceleration structure for winding-number evaluation based

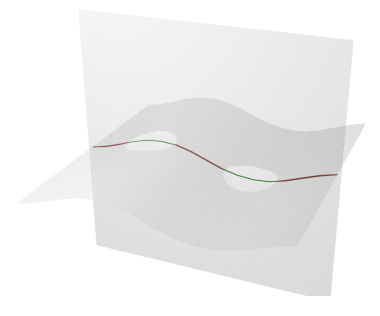


Fig. 3. Topological intersection between two faces. Extraneous portions of the intersection curve must be removed using point–surface containment queries.

on ellipse bounds of Bézier curves, and extend the formulation to periodic domains by lifting the computation to the universal covering space.

Our main contributions are as follows:

- We introduce a novel recursive scheme that accelerates windingnumber evaluation by bounding Bézier segments with ellipse regions, avoiding $O(n^2)$ curve subdivision and achieving linear-time complexity.
- We formulate containment queries on periodic surfaces in the universal covering space, enabling robust computation for loops that are non-contractible or discontinuous in parameter domain.
- We demonstrate the use of our algorithm for robust tessellation of trimmed surfaces and interactive design of complex periodic geometries.

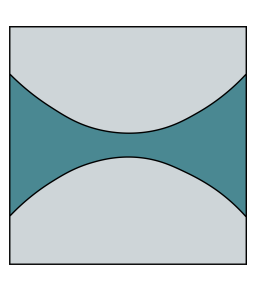
The remainder of this paper is organized as follows. Section 2 reviews previous work on containment queries and curve evaluation. Section 3 presents the preliminaries. Section 4 details the proposed winding-number computation and its extension to periodic domains. Section 5 reports experimental comparisons and applications. Section 6 discusses limitations and directions for future work, and Section 7 concludes the paper.

2 RELATED WORK

2.1 Containment Queries for Non-Parametric Boundaries

We first review containment query methods developed for *non-parametric* geometries such as line segments, polygons, and triangular meshes. These problems have been extensively studied in the computer graphics community, primarily through two families of techniques: ray casting and winding number computation.

Ray casting. Ray casting is the most widely used approach for point-in-solid classification, both in two-dimensional polygons and three-dimensional meshes. The method shoots a ray from the test point in a fixed direction and counts intersections with the object boundary. By the Jordan curve theorem, an odd number of crossings indicates an interior point, while an even number indicates an exterior one.





Parameter Domain

Physical Space

Fig. 4. A periodic trimmed surface defined on a cylindrical geometry. The boundary consists of two separation loops, which do not form closed loops in the parameter domain.

Ray casting can be accelerated through spatial data structures such as KD-trees and bounding volume hierarchies (BVH) [Goldsmith and Salmon 1987; Rubin and Whitted 1980]. For rendering purposes, modern frameworks also support GPU acceleration and parallel ray traversal [Parker et al. 2010].

Despite its success in photo-realistic rendering, ray casting suffers from robustness issues in geometry processing. It fails for open or non-manifold boundaries, since the Jordan theorem applies only to closed curves. In practice, ray-casting failures often occur at degenerate intersections, coincident edges, or geometric inconsistencies (Figure 5). A common workaround is to shoot multiple rays in random directions, which increases computational cost.

Winding number methods. Winding numbers provide a robust alternative to ray casting by offering a continuous measure of containment. Jacobson et al. [2013] introduced the generalized winding number to handle open boundaries robustly. Barill et al. [2018] extended this idea to point clouds, and Sun et al. [2024] defined a differentiable version based on Gaussian smoothing. Most relevant to our work, Feng et al. [2023] formulated the surface winding number (SWN) as a solution to a boundary value problem with a jump condition, enabling manifold-aware containment queries. However, this approach requires solving a global linear system, which is inefficient for local or single-point queries.

Compared to ray casting, winding-number-based methods are more robust in the presence of geometric errors, open boundaries, and non-manifold configurations. Spatial acceleration structures for non-parametric geometries have also been explored [Barill et al. 2018; Jacobson et al. 2013], but analogous data structures for parametric geometries remain underdeveloped.

2.2 Containment Queries for Parametric Boundaries

We now discuss methods for containment queries involving curved parametric boundaries, such as Bézier or NURBS curves.

Ray casting. Containment queries on trimmed surfaces are typically solved by ray-casting-based methods. The main computational challenge lies in computing the intersection between a ray and a curve, which reduces to finding the roots of a polynomial expressed in the Bernstein basis. Nishita et al. [1990] introduced the Bézier

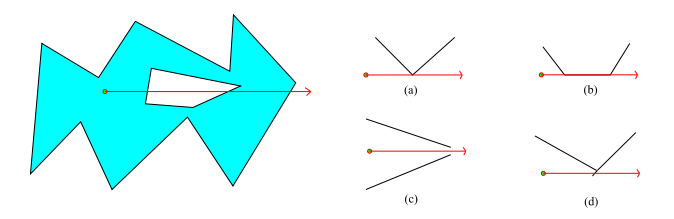


Fig. 5. Ray casting and its failure cases. Left: The classic even-odd rule determines inside/outside classification by counting ray-boundary intersections. Right: Common failure cases include (a) invalid intersection points, (b) rays coincident with boundary segments, (c) open boundaries due to geometric errors, and (d) non-manifold configurations.

clipping algorithm, which exploits the control polygon to isolate root intervals. Subsequent works improved its convergence rate, such as quadratic clipping [Bartoň and Jüttler 2007] and cubic clipping [Liu et al. 2009]. The current state-of-the-art is the Bézier zero factoring method [Machchhar and Elber 2016], which reduces polynomial degree by exploiting factorization properties of Bernstein polynomials, achieving superior efficiency.

Curve hierarchical schemes. To accelerate repeated ray-curve queries, hierarchical structures have been developed for Bézier curves. Most are based on identifying monotone segments or local extrema to form spatial subdivisions.

Earlier data structures include the arc tree [Günther and Wong 1990], which uses arc-length parameterization, and the strip tree [Ballard 1981], which bounds curve segments with rectangles. Schollmeyer and Fröhlich [2009] proposed splitting trimming curves into monotone pieces to avoid root finding. Schollmeyer and Froehlich [2018] introduced KD-tree-based spatial subdivision, while Sloup and Havran [2021] refined KD-tree construction for faster point location. For Bézier curves, recursive control-point hierarchies remain the most widely used strategy.

Winding number methods. All methods relying on crossing counts are inherently sensitive to geometric errors such as open or nonmanifold boundaries. While repair techniques exist, such issues are still pervasive in CAD and B-Rep models. Spainhour et al. [2024] proposed a robust containment method for parametric curves using the generalized winding number. Our method builds upon this line of work but introduces an ellipse bound for faster Bézier evaluation and bound inclusion tests, as well as a complete treatment of periodic domains. Liu et al. [2025] formulated winding-number computation through complex polynomial roots, and Martens and Bessmeltsev [2025] developed a hybrid approach combining ray casting with winding evaluation. Spainhour and Weiss [2025] further extended winding numbers to trimmed surfaces; their focus is on determining whether a point lies inside a solid defined by trimmed surfaces, while our work focuses on classifying points on the trimmed surface itself.

Periodic surfaces. Periodic surfaces are pervasive in CAD, including cylinders, tori, and spheres, all of which have periodic parameter domains (see Figure 2). Such periodicity causes difficulties for both ray casting and winding-number-based methods, as trimming

curves may cross domain boundaries or appear artificially open. To our knowledge, no prior work provides a systematic solution for containment queries on trimmed surfaces with periodic parameterizations. Feng et al. [2023] partially addresses periodicity, but only for non-parametric geometries and via global linear solves.

3 PRELIMINARIES

3.1 Boundary Representation and Trimmed Surfaces

Boundary representation (B-Rep) is the de facto international standard [Pratt et al. 2001] for representing parametric CAD models. In B-Rep, a solid entity is defined by its boundaries. To represent the boundary of complex solids, flexible free-form surfaces are required, and the most common choice is trimmed non-uniform rational B-spline (NURBS) surfaces.

A NURBS surface is described by a control net and defines a smooth mapping from a (possibly periodic) parameter domain, usually $[0,1] \times [0,1]$, to physical space \mathbb{R}^3 . To represent surfaces with non-zero genus, a set of curves $\{\gamma_i\}$ is defined on the surface to trim it, yielding the concept of a **trimmed surface**. A trimmed surface consists of a parametric surface patch (typically a NURBS surface) and a set of boundary curves γ_i . The projection of these boundary curves onto the parameter domain is referred to as the **p-curves**.

Mathematically, a trimmed surface can be completely specified by its geometric and topological data even without the p-curves. However, for computational efficiency in tasks such as tessellation or containment queries, p-curves are an essential component of B-Rep models. They can be obtained by sampling, inverting, and subsequently fitting the results with Bézier or NURBS curves. For further discussion on p-curve computation, we refer readers to Flöry and Hofer [2008]; Hofer and Pottmann [2004]; Renner and Weiss [2004]. P-curves also naturally arise in surface–surface intersections computed via marching methods [Barnhill and Kersey 1990]; see Marussig and Hughes [2018] for a comprehensive review of intersection and trimming techniques.

In this paper, the p-curves are represented by (rational) Bézier or NURBS curves. For simplicity, we focus on the Bézier case; the rational case is discussed in Appendix A.1. B-spline or NURBS curves can always be subdivided into (rational) Bézier segments [Farin 2001].

Curves on general surfaces can exhibit significant geometric complexity, but in computer graphics and CAD, the discussion is simplified by the topological constraints of spline parameterizations. Modern CAD systems parameterize surfaces via mappings from rectangular domains $[a,b] \times [c,d]$ to \mathbb{R}^3 . Cylinder-like or torus-like surfaces are represented using periodic parameter domains. Herron [1985] proved that smooth spline surfaces cannot represent shapes of genus greater than one. Consequently, a single spline patch is topologically equivalent to a disk, sphere, cylinder, or torus—all of which can be covered by periodic domains. To represent surfaces of higher genus, multiple patches must be employed.

3.2 Generalized Winding Number

The winding number has long been used in computer graphics. Jacobson et al. [2013] introduced the *generalized winding number* for

robust inside/outside classification. For a closed curve γ parameterized by $t \in [0,1]$ and a fixed point p, the winding number $\omega(p,\gamma)$ is defined as

$$\omega(p,\gamma) = \frac{1}{2\pi} \int_{\gamma-p} d\theta,$$

where θ is the polar angle with respect to the positive *x*-axis.

By definition, the winding number has an important property: it is *additive*. If $\gamma = \gamma_1 + \gamma_2$ (defined by concatenation), then

$$\omega(p,\gamma) = \omega(p,\gamma_1) + \omega(p,\gamma_2). \tag{1}$$

From the viewpoint of algebraic topology, the winding number is also *homotopy invariant*. If γ and $\bar{\gamma}$ are homotopy equivalent in $\mathbb{R}^2 \setminus \{p\}$ (with the test point removed), then

$$\omega(p,\gamma) = \omega(p,\bar{\gamma}). \tag{2}$$

Intuitively, the winding number remains unchanged under any continuous deformation of γ that does not cross the test point p.

Using this property, if γ lies within a simply connected region Ω and $p \notin \Omega$, then

$$\omega(p,\gamma) = \omega(p,\gamma(0),\gamma(1)),\tag{3}$$

where $\omega(p,a,b)$ denotes the winding number of the oriented segment \overrightarrow{ab} with respect to p, computed from its angular difference. These two properties form the foundation of our method as well as of previous winding-number–based approaches [Spainhour et al. 2024].

3.3 Homology of Loops on a Torus

To precisely describe our winding-number algorithm on periodic domains and explain its correctness, we employ the language of homology. For readers unfamiliar with homology theory, a loop on a torus with homology coefficients (p,q) can be understood geometrically as one that wraps p times around one periodic direction of the surface (for example, the longitudinal direction) and q times around the other (the meridional direction). In the corresponding universal covering space—which unfolds the periodic surface into an infinite planar tiling—this loop no longer closes onto itself; instead, its start and end points differ by a translation of (p,q) units. Loops with coefficients (0,0) are contractible on the original surface, whereas nonzero coefficients indicate loops that cross periodic boundaries. For a formal and rigorous treatment of homology from the perspective of algebraic topology, we refer readers to Munkres [2018].

4 METHOD

In this section, we first outline our containment query algorithm and introduce the *ellipse bound*, which avoids expensive curve subdivision (Section 4.2). We then discuss periodic parameterizations in CAD systems and interpret them in terms of universal covering spaces (Section 4.3). Building on this, Section 4.4 establishes winding number primitives for periodically extended curves, and Section 4.5 describes the complete winding number algorithm for uni- and bi-periodic domains.

For convenience, we assume the parameter domain of the surface is $D = [0, 1] \times [0, 1]$, and all curve parameters vary within [0, 1].

4.1 Algorithm Overview

Given a test point p and a set of trimming curves $\{\gamma_i\}$, our goal is to determine whether p lies within the trimmed region. We do this by computing the winding number of the trimming curves with respect to p, and then classifying p as inside or outside based on this value.

As discussed in Section 3.2, the winding number is both additive and homotopy invariant. Thus, for each trimming curve, if we can enclose it within a convex region in the parametric domain, then for any test point outside this region, the curve can be replaced by a straight line segment without affecting the winding number. For test points inside the region, we subdivide the curve at its midpoint, compute new bounds for the two subsegments, and apply the same process recursively. In the recursion, if we detected that the distance between p and current endpoints is smaller than a predefined tolerance ϵ , the point is reported as lying on the boundary. Note that not all points within the ϵ -shell of boundary curves are labeled on-boundary, since points that can be confidently classified as inside or outside are excluded.

The outline of the recursive winding number computation is shown in Algorithm 1. The two main primitives are (1) how to bound a Bézier segment, and (2) how to classify whether a point lies inside the bound.

Algorithm 1 ComputeWindingNumber

```
Require: Test point p, 2D parametric Bézier curve \gamma, interval [a, b],
     tolerance \epsilon
Ensure: Winding number \omega(p, \gamma_{[a,b]})
     if d(p, \gamma(a)) < \epsilon or d(p, \gamma(b)) < \epsilon then
          Return on-boundary
     else if p not in bound of \gamma_{[a,b]} then
          \omega \leftarrow WindingNumberLineSegment(p, \gamma(a), \gamma(b))
     else
           m \leftarrow (a+b)/2
          \omega_1 \leftarrow ComputeWindingNumber(p, \gamma, a, m, \epsilon)
          \omega_2 \leftarrow ComputeWindingNumber(p, \gamma, m, b, \epsilon)
          \omega \leftarrow \omega_1 + \omega_2
     end if
```

4.2 Ellipse Bound

Let γ be a Bézier curve defined by control points $\{P_i\}_{i=0}^n$. It is well known that the convex hull of the control points bounds the curve. However, using this bound in each recursion requires invoking De Casteljau's algorithm to subdivide the curve and update the control points of each split. For containment tests, a point-in-polygon query is also needed. This results in $O(n^2)$ cost for curve subdivision and O(n) for point-in-bound tests.

To reduce this cost and enable efficient geometric primitives such as Woźny and Chudy [2020], we propose an ellipse bound that replaces the convex-hull test with a simple analytic condition.

LEMMA 4.1 (Ellipse Bound). Every (rational) Bézier curve y lies within the ellipse region Ω_V defined by

$$\Omega_{Y} = \{ x \in \mathbb{R}^{2} \mid d(x, P_{0}) + d(x, P_{n}) \leq B \},$$
 (4)

where B is an upper bound on the curve's derivative magnitude. For a non-rational Bézier curve, $B = \max_i ||n(P_i - P_{i-1})||$. The rational case is given in Appendix A.1.

The proof follows directly from the Lipschitz bound of Bézier derivatives and is provided in Appendix A.1. Conceptually, this bound defines an ellipse whose foci are the curve's endpoints, and whose major axis is determined by the curve's maximum derivative. This ellipse fully encloses the curve.

For a subsegment $\gamma': [a,b] \to \mathbb{R}^2$, the corresponding bound becomes

$$\Omega_{\gamma'} = \{ x \in \mathbb{R}^2 \mid d(x, \gamma(a)) + d(x, \gamma(b)) \le B(b - a) \}.$$
 (5)

This formulation enables the recursive winding number algorithm to test containment using only the endpoints of the curve—avoiding both De Casteljau subdivision and point-in-polygon queries—thereby improving performance while keeping numerical robustness.

With the ellipse bound, the termination of Algorithm 1 can be guaranteed which is formally described by following lemma and proved in Appendix A.2.

LEMMA 4.2 (TERMINATION). The maximum recursion depth in Algorithm 1 is

$$O\left(\log \frac{B}{\max(\epsilon, d)}\right),$$

where ϵ is the geometric tolerance, d is the distance between the test point p and the curve γ , and B is the bound constant same with the Equation 4.

In practice, far fewer subdivisions are needed, since most subsegments are pruned during recursion. Empirically, the average runtime grows logarithmically with respect to $1/\epsilon$ for boundary-adjacent test points.

Path hierarchy. Beyond single curves, we define a path as a sequence of end-to-end continuous Bézier segments $\{\gamma_i\}_{i=1}^n$. An ellipse bound for any subpath $\{\gamma_i\}_{i=j}^k$ can be written as

$$\Omega_{j,k} = \big\{x \in \mathbb{R}^2 \; \big| \; d(x,\gamma_j(0)) + d(x,\gamma_k(1)) \leq \max_{j \leq m \leq k} B_m(k-j+1) \,\big\}.$$

This hierarchical structure enables efficient pruning in both CAD and vector graphics applications. For example, a NURBS curve can be decomposed into rational Bézier segments, and a hierarchy of ellipse bounds can be built for fast containment queries.

Table 1 compares the computational cost of the ellipse bound versus the traditional control-points bound. The ellipse bound reduces evaluation and in-bound testing from $O(n^2)$ and O(n) to O(n)and O(1), respectively. A similar hierarchy can also be evaluated in constant time. We note that concurrent work by Woźny and Chudy [2025] proposed a stable $O(n \log n)$ subdivision method based on the Fast Fourier Transform, but it applies only to non-rational Bézier curves; rational curves still require $O(n^2)$ subdivision.

Relation to arc trees. Our ellipse bound differs from that used in arc trees [Günther and Wong 1990], which rely on arc length. Computing arc-length parameterizations for general Bézier curves is often intractable [Sakkalis et al. 2009], making our derivative-based ellipse bound more practical for CAD applications.

Table 1. Comparison of computational cost between ellipse bounds and control-points bounds, where n is the number of control points.

	Ellipse Bound	Control-Points Bound	
Evaluation	O(n)	$O(n^2)$	
In-bound Test	O(1)	O(n)	
Path Hierarchy	O(1)	O(n)	

4.3 Periodic Surfaces and Their Covering Space

Periodic parameterizations are ubiquitous in CAD models. Seamless cylinders, tori, and their deformations are represented by surfaces whose parameter domains are periodic rectangles. From a topological viewpoint, such surfaces fall into three main categories:

- Cylinder-like: represented by a uni-periodic domain.
- Torus-like: represented by a bi-periodic domain.
- Sphere or cone-like: represented by a uni-periodic domain with one or more singular points.

For surfaces homeomorphic to the sphere or cone, we can puncture the singular points, effectively reducing them to the cylinder-like case.

Evaluating the winding number directly in the parameter domain is problematic because trimming curves may cross the domain boundary or appear artificially open due to periodic identification. To address this, we interpret trimming loops within the viewpoint of the *universal covering space*.

The universal covering space of a uni- or bi-periodic rectangle is the infinite plane, tiled by translated copies of the base domain. Tiles repeat along one axis for uni-periodic domains and along both axes for bi-periodic domains. In this lifted space (Figure 6):

- Contractible loops remain contractible.
- Non-contractible loops lift to periodically extended curves, which repeat infinitely across tiles.

This perspective transforms boundary-crossing trimming curves into well-defined entities whose winding numbers can be computed consistently.

4.4 Periodically Extended Curves

We now formalize the concept of periodically extended curves and show how to compute their winding numbers. The key idea is to truncate the infinite set of copies: segments sufficiently far from the query point can be replaced by straight lines without changing their contribution.

Definition. Let $\gamma : \mathbb{R} \to \mathbb{R}^2$ be a curve, and assume there exists a period $T \in \mathbb{R}$ such that

$$\gamma(t+T) = \gamma(t) + \vec{v},\tag{6}$$

for some nonzero translation vector $\vec{v} \in \mathbb{R}^2$. We call γ a periodically extended curve with extension vector \vec{v} . We partition γ into unit segments:

$$\gamma_n: [0,T] \to \mathbb{R}^2, \qquad \gamma_n(t) = \gamma(nT+t).$$

Let $\beta_n = \gamma_n(0)$; all β_n lie on a line L parallel to \vec{v} . The winding number of γ with respect to a test point p can be written as an

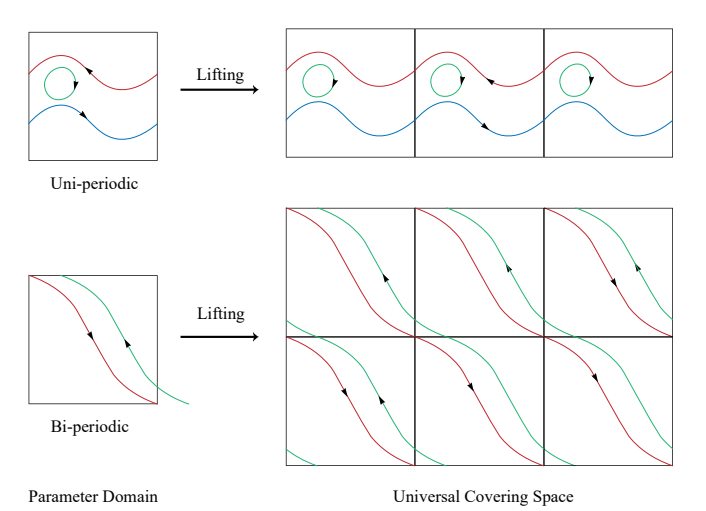


Fig. 6. Universal covering spaces of periodic domains. Contractible loops lift to closed loops, while non-contractible loops become periodically extended curves that repeat across tiles.

infinite series:

$$\omega(p,\gamma) = \sum_{k=-\infty}^{\infty} \omega(p,\gamma_k). \tag{7}$$

Although Equation (7) is not directly computable, the convergence is effectively finite. Since $\|\vec{v}\| > 0$, there exists N such that for all |k| > N, the ellipse bounds of γ_k do not contain p. By homotopy invariance, the contributions from these distant copies can be replaced by straight segments between β_k and β_{k+1} . Hence,

$$\omega(p,\gamma) = \sum_{k=-N}^{N} \omega(p,\gamma_k) + \sum_{|k|>N} \omega(p,\gamma_k)$$

$$= \sum_{k=-N}^{N} \omega(p,\gamma_k) + \sum_{|k|>N} \omega(p,\beta_k,\beta_{k+1})$$

$$= \sum_{k=-N}^{N} \omega(p,\gamma_k) + \omega(p,L) - \omega(p,\beta_{-N},\beta_{N+1}).$$
(8)

Here $\omega(p,L)$ denotes the winding number of the infinite line L with respect to p, computed by a simple left–right test: if p lies on the left side of L, $\omega(p,L)=1/2$; otherwise, $\omega(p,L)=-1/2$. The final correction term $\omega(p,\beta_{-N},\beta_{N+1})$ subtracts the spurious contribution of the long chord spanning the truncated region. Figure 7 illustrates this construction.

In practice, only a small number of local segments of γ need to be evaluated using the recursive ellipse-bound algorithm. All remaining copies reduce to a single straight-line contribution. This approach ensures that winding number queries on periodic domains remain robust, efficient, and mathematically consistent.

4.5 Periodic Domain

With the framework described in Section 4.4, containment queries on a *uni-periodic* domain can be solved directly. Let the tiles of the

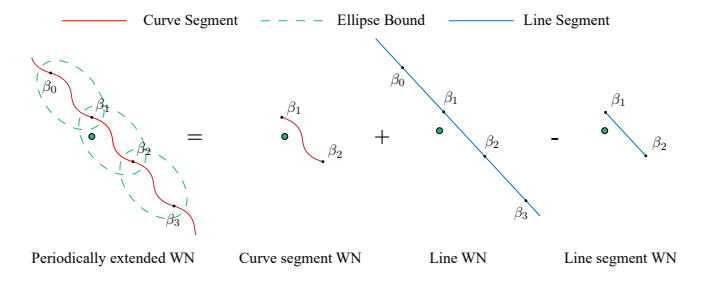


Fig. 7. Winding number computation for a periodically extended curve. Nearby copies of y are evaluated using the standard winding number primitive, while distant copies are replaced by straight-line contributions.

universal covering space be denoted by D_n , where $n \in \mathbb{Z}$. For a trimming loop γ , two cases arise:

- Contractible loop: γ lifts to closed loops $\gamma_n = \gamma + n\vec{e}_1$. In this case, components that are far from the test point can be safely discarded.
- Non-contractible loop: the lifted copies of γ form a periodically extended curve, and its winding number can be computed using the primitives introduced in Section 4.4.

When the domain is *bi-periodic*, the situation becomes more subtle. Each loop γ is lifted to

$$\gamma + i\vec{e}_1 + j\vec{e}_2, \qquad i, j \in \mathbb{Z}.$$

Unlike the uni-periodic case, even a contractible loop now has infinitely many lifted copies. A naive summation of winding numbers,

$$\omega(p, \{\gamma_i\}_{1 \le i \le n}) = \sum_{i = -\infty}^{\infty} \sum_{j = -\infty}^{\infty} \sum_{k = 1}^{n} \omega(p, \gamma_k + i\vec{e}_1 + j\vec{e}_2), \qquad (9)$$

is not absolutely convergent. We therefore develop another way to properly formulate the winding number.

Key ideas. We observe that the trimming loops on a torus-like surface must adhere to topological constraints. In particular, noncontractible loops must appear in oppositely oriented pairs with the same homology coefficients. Each such pair defines a band-like region in the universal covering space—an infinitely repeating but finite-width strip. The winding number over the entire domain can then be defined as the sum of contributions from these bands, and only a finite number of bands near the test point need to be considered. Figure 8 shows the overall motivation of proposed algorithm on bi-periodic domain via a simple example.

The following proposition provides the topological foundation for our approach.

Proposition 4.3. Let S be a surface smoothly parametrized by a bi-periodic mapping to \mathbb{R}^3 , and let $\gamma_1, \gamma_2, \ldots, \gamma_n$ be disjoint, selfintersection-free loops on S that together define a bounded region on S, i.e., $\gamma_1 + \cdots + \gamma_n$ is null-homologous. Then, the set $\{\gamma_i\}$ can be partitioned as

$$\{\gamma_i\} = A \cup B \cup C,\tag{10}$$

where A contains all loops with homology coefficients (p, q), B contains those with -(p,q), and C contains all contractible loops. Moreover, A and B have the same cardinality.

Intuitively, Proposition 4.3 implies a strong structural restriction on trimming loops in a torus-like parameter domain: all noncontractible loops must appear in oppositely oriented pairs with identical homology coefficients. This allows us to group the loops into pairs (α, β) with $\alpha \in A$ and $\beta \in B$, and each pair (α, β) defines a band-like region in the universal covering space. A formal proof is provided in Appendix B.1.

To compute the winding number contributed by a pair (α, β) , we must enumerate all their lifted copies. The following proposition shows how to partition the set of all lifted copies of a loop with homology coefficients (p, q) into a family of periodically extended curves. Proof is provided in Appendix B.2

Proposition 4.4. For a loop y with homology coefficients (p,q), the set of all its lifted copies $\{\gamma + i\vec{e}_1 + j\vec{e}_2\}_{i,j\in\mathbb{Z}}$ can be partitioned into disjoint periodically extended curves:

$$\bigcup_{i=-\infty}^{\infty} \bigcup_{j=-\infty}^{\infty} (\gamma + i\vec{e}_1 + j\vec{e}_2) = \bigcup_{r=0}^{p-1} \bigcup_{s=-\infty}^{\infty} \gamma_{r,s}, \tag{11}$$

where $\gamma_{r,s}$ is defined as

$$\gamma_{r,s} = \sum_{l=-\infty}^{\infty} (\gamma + (r+pl)\vec{e}_1 + (s+ql)\vec{e}_2), \quad 0 \le r \le p-1, \ s \in \mathbb{Z}.$$
 (12)

Now, consider a pair of loops α and β with homology coefficients (p,q) and -(p,q), respectively. Their lifted copies $\alpha_{i,j}$ and $\beta_{i,j}$ bound infinitely repeating band-like regions in the covering space. The winding number of this pair is defined as

$$\omega(p, \{\alpha, \beta\}) = \sum_{i=0}^{p-1} \sum_{j=-\infty}^{\infty} \left(\omega(p, \alpha_{i,j}) + \omega(p, \beta_{i,j}) \right). \tag{13}$$

As illustrated in Figure 8, only finitely many of these bands intersect the base domain $[0,1] \times [0,1]$, so the summation reduces to a finite set of terms. Each term $\omega(p, \gamma_{i,j})$ can be evaluated efficiently using the primitives described in Section 4.4.

Summary. By enumerating all loop pairs in *A* and *B* (as defined in Proposition 4.3) and summing their contributions according to Equation (13), we obtain the total winding number for all non-contractible loops. The complete pairing algorithm, including pseudo-code and special cases, is provided in Appendix C. Although the derivation assumes continuous and disjoint loops, the method remains robust under typical geometric imperfections, such as disconnected or overlapping p-curves (see Figure 1).

EXPERIMENTATION

5.1 Implementation

We implemented the proposed algorithm in C++, and all experiments were executed on a single thread. Runtimes were measured on a PC equipped with an Intel Core i9-13900HX CPU and 32 GB of RAM.

5.2 2D Containment Query with Parametric Boundaries

We first evaluate the proposed winding number algorithm on planar containment queries for parametrically represented curves in a simply connected domain.

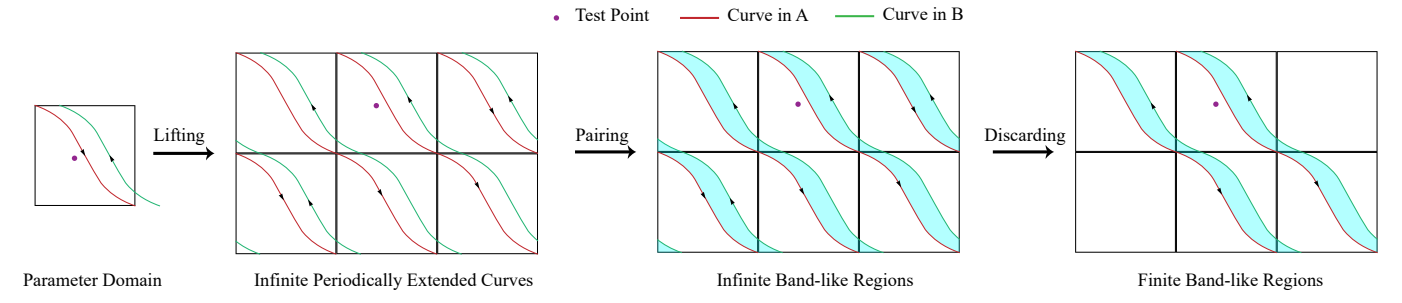


Fig. 8. Pipeline of our algorithm on a bi-periodic domain. Following Proposition 4.3, the p-curves are divided into two sets, *A* and *B*. Lifting them to the universal covering space yields infinite periodically extended curves, which are paired to form band-like regions. Regions far from the test point are discarded, and winding numbers are computed using the primitives described in Section 4.4.

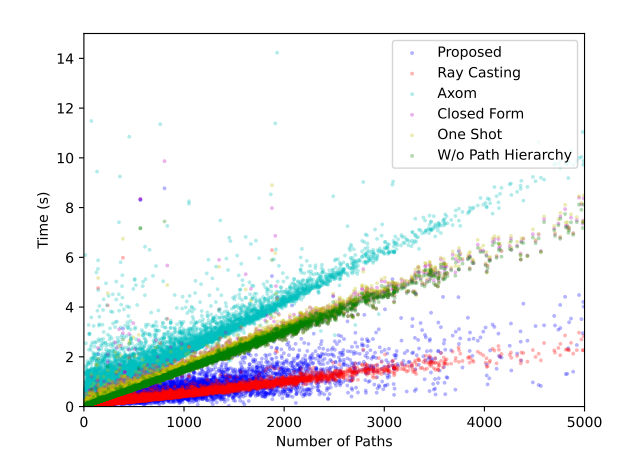


Fig. 9. Runtime comparison across methods on the OpenClipArt20K dataset [Hu et al. 2019]. Extremely large or small values are clipped for readability. The proposed method achieves performance comparable to non-robust ray casting and significantly outperforms recent robust winding number approaches such as Axom [Spainhour et al. 2024].

5.2.1 Performance. We compare our method with both ray-casting and winding number algorithms, including Axom [Spainhour et al. 2024], ClosedForm [Liu et al. 2025], and OneShot [Martens and Bessmeltsev 2025]. For the ray-casting baseline, we adopt the pruning strategy of Nishita et al. [1990] and use a state-of-the-art Bézier root solver [Machchhar and Elber 2016]. The default ray direction is along the positive u-axis.

We evaluate performance on two datasets: the OpenClipArt20K dataset [Hu et al. 2019] and the publicly available Bézier Guarding (BG) dataset [Mandad and Campen 2020]. OpenClipArt20K consists of 20,000 SVG files containing both simple and highly complex shapes. We extract the Bézier paths from each SVG, normalize them to the unit square $[0,1] \times [0,1]$, and treat them as shape boundaries. The BG dataset includes four categories of randomly generated Bézier curves, as illustrated in Figure 11. For OpenClipArt20K, we preserve the original SVG path hierarchy, whereas for the BG dataset, we also evaluate our method without hierarchy acceleration. For

each shape, 256×256 sample points are uniformly distributed across the parametric domain, and all algorithms are evaluated under identical settings.

Table 2 reports the average runtime, and Figure 9 shows the runtime distribution on OpenClipArt20K. Compared to Axom [Spainhour et al. 2024], our method significantly accelerates winding number computation, reducing runtime to **27.3%** of Axom's on real-world SVG shapes. The performance is also comparable to the optimized, yet non-robust, ray-casting method [Nishita et al. 1990]. For BG subsets A and B, both methods perform similarly, while on subsets C and D, the pruning strategy in [Nishita et al. 1990] gives ray casting a strong advantage due to the sparse distribution of curves.

Table 2. Average runtime (seconds) of different algorithms on OpenClipArt20K [Hu et al. 2019] and BG [Mandad and Campen 2020] datasets. Our method reduces winding number computation time to 27.3% of Axom's [Spainhour et al. 2024] while achieving performance comparable to an optimized ray-casting approach.

sed
7
5
4
1
4

As an ablation study, Figure 9 also reports performance without the path hierarchy. The hierarchy significantly accelerates winding number computation, particularly for complex shapes. In such cases, the benefit of linear evaluation becomes less pronounced, as all boundaries are cubic Bézier curves.

We further analyze the asymptotic behavior of different algorithms. Using the BG Dataset A [Mandad and Campen 2020], we elevate cubic curves to higher degrees without altering geometry. Test points are sampled directly from the boundary—the worst case for recursive methods such as ours and Spainhour et al. [2024]. Figure 12 shows that our algorithm demonstrates empirically linear asymptotic behavior, while the control-point-based method exhibits faster growth in runtime.

We also evaluate the effect of tolerance ϵ using BG Dataset A. Our algorithm is tested under uniform sampling and on-boundary

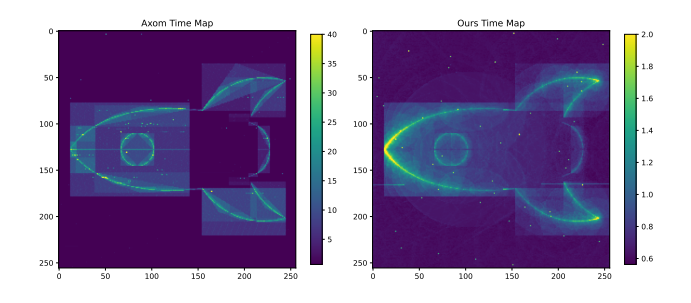


Fig. 10. Spatial distribution of runtime cost for Axom and the proposed method on the parameter domain. Different colormaps are used for clarity: the left ranges from 0-40 ms and the right from 0-2 ms. The proposed method exhibits more uniform performance across the domain.

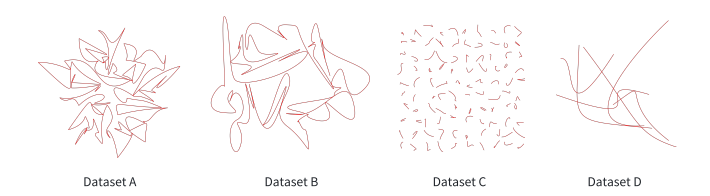
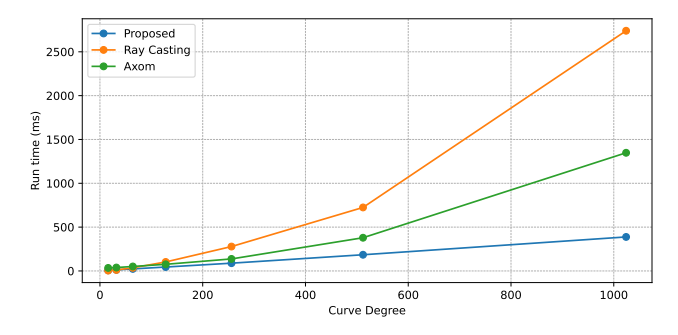


Fig. 11. Examples from the Bézier Guarding dataset [Mandad and Campen 2020]. Dataset A: Closed C^0 boundaries. Dataset B: Closed C^1 boundaries. Dataset C: Isolated random curves uniformly distributed across the domain. Dataset D: Randomly intersecting curves.

Fig. 12. Runtime versus boundary degree for different algorithms. The proposed method exhibits empirically linear scaling, while the control-pointbased approach [Spainhour et al. 2024] grows faster with increasing curve order



sampling. Table 3 lists the runtime and the number of curve evaluations for each tolerance value. Uniform sampling shows negligible dependence on ϵ , while boundary sampling exhibits an empirical logarithmic trend. Figure 10 visualizes the global distribution of computational cost.

5.2.2 Robustness. From a robustness perspective, ray casting fails even on simple shapes with minor geometric inconsistencies. As shown in Figure 14, both methods perform correctly on clean, closed

Table 3. Effect of tolerance ϵ on performance. Runtime (in seconds) and number of curve evaluations for classifying 1 million points on BG Dataset A, under uniform and on-boundary sampling. The results demonstrate the method's robustness and its logarithmic dependence on ϵ for boundaryadjacent points.

ϵ	10^{-4}	10^{-5}	10^{-6}	10^{-7}	10^-8
Boundary eval count	35.95	45.02	54.18	63.41	72.46
Boundary time (ms)	2.60	2.95	3.26	3.68	4.05
Uniform eval count	16.22	16.28	16.29	16.29	16.29
Uniform time (s)	0.086	0.090	0.091	0.090	0.086

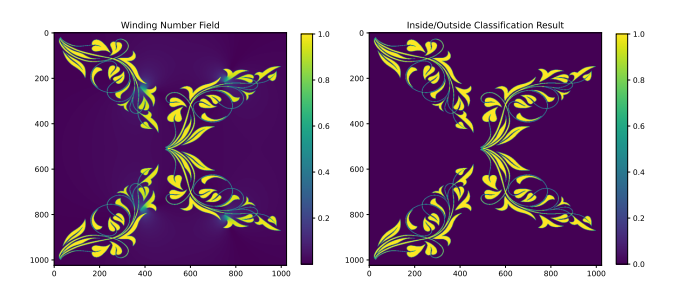


Fig. 13. An extremely complex shape from OpenClipArt (ID = 237213). Some boundary curves are missing, yet the winding number classification automatically corrects these geometric errors.

shapes. However, when random noise is added to boundary control points—introducing non-manifold or open boundaries—the raycasting approach fails, while winding number methods remain stable. Figure 13 further demonstrates that our method can handle extremely complex open-boundary shapes, automatically repairing gaps through the topological consistency of the winding number.

5.2.3 Correctness and Accuracy. To assess accuracy and numerical stability, we applied the proposed containment-query algorithm to BG Dataset A under varying tolerance values. Results are shown in Figure 15. As ϵ decreases, the fraction of points classified as on-boundary quickly approaches zero. For all points confidently classified as inside or outside, the maximum deviation in winding number is 3.95×10^{-9} relative to the ground truth computed by Liu et al. [2025].

5.3 Periodic Domain

In this section, we evaluate the proposed algorithm on periodic domains. Unlike the simply connected case, regions in a periodic domain may have non-closed boundaries. Although conventional winding-number methods can tolerate small geometric inconsistencies such as open boundaries, they still fail on many periodic configurations—examples of which were already shown in Figure 13.

Using the formulation presented in Section 4.5, we can efficiently and correctly compute winding numbers in periodic domains. As illustrated in Figure 16, directly applying conventional winding number evaluation for inside/outside classification fails for both

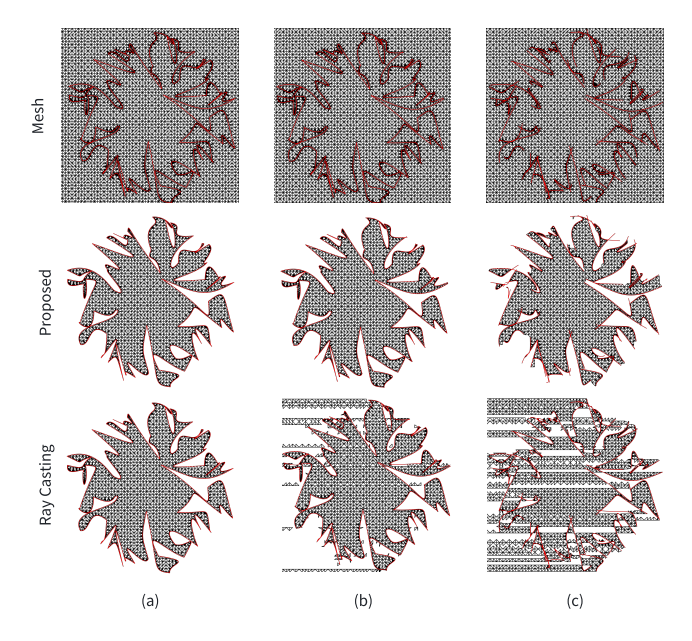


Fig. 14. Robustness comparison using BG Dataset A (ID = 694). The boundary is discretized and the domain triangulated via constrained Delaunay triangulation; containment queries are performed at triangle barycenters. (a) Closed boundary: both methods succeed. (b-c) Boundaries perturbed with Gaussian noise $\mathcal{N}(0,10^{-3})$ and $\mathcal{N}(0,10^{-2})$. Ray casting fails under non-manifold or open boundaries, whereas the winding number remains stable.

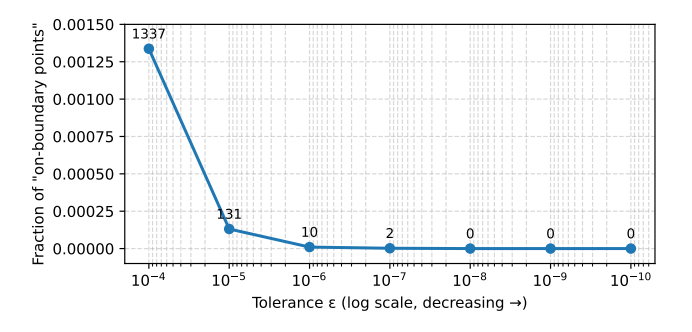


Fig. 15. Fraction of points reported as on-boundary among 10^6 uniformly sampled test points, for different tolerance values ϵ . Each marker is annotated with the number of boundary detections. As ϵ decreases from 10^{-4} to 10^{-10} , the ambiguous fraction rapidly vanishes—from 0.13% to 0%.

non-closed p-curves and curves crossing domain boundaries. In such cases, directly computed winding number often misclassifies points on the trimmed surface as "outside," and regions crossing periodic boundaries are lost. In contrast, our periodic formulation correctly handles both non-closed and boundary-crossing p-curves, preserving the complete trimmed surface.

To further assess the correctness and performance of the periodic winding-number algorithm, we constructed a synthetic dataset consisting of two parts:

- Dataset A: Non-contractible loops in a uni-periodic domain.
- **Dataset B:** Non-contractible loops in a bi-periodic domain with homology coefficients satisfying $2 \le p, q \le 5$.

Figures 24 and 25 visualize the computed winding numbers for both datasets. Compared with direct evaluation, our periodic formulation yields correct and topologically consistent results in all cases.

5.4 Application

5.4.1 Processing Multiple Patches. We demonstrate our method on boundary representation (B-Rep) models consisting of multiple surface patches. As illustrated in Figures 19 and 20, we construct B-Rep models by applying Boolean union operations between solids, resulting in multi-patch surfaces. Sample points are generated on the original geometric surfaces, and containment queries are then used to determine whether each point lies on the newly formed faces.

For a sample point p on a geometric surface S, containment is determined by testing p against all trimmed surfaces referencing S as their base geometry. If p lies within any trimming loop, it is labeled as inside; otherwise, it is classified as outside. Figure 21 further shows results on real-world CAD models. Even for complex configurations, our method robustly identifies points trimmed away by face boundaries.

- 5.4.2 B-Rep Intersection. We demonstrate the application of the proposed algorithm to boundary representation (B-Rep) intersection, a fundamental modeling operation in CAD systems. The input consists of two B-Rep solids, and the goal is to compute the set of intersection curves between them. This process typically involves two stages:
 - Geometric intersection: computing intersection curves between the underlying untrimmed surfaces of the two solids, often using the marching method [Barnhill and Kersey 1990].
 - **Topological intersection:** filtering the raw geometric intersections using the trimming boundaries of each surface to retain only the valid segments.

In the second stage, intersection curves are segmented by the trimming boundaries of the participating surfaces. To determine whether each resulting segment lies within the trimmed region, we evaluate a point containment query at its midpoint.

Figure 17 illustrates an example where an "eight"-shaped surface (genus two, represented by four torus patches) intersects with a wave surface. Stage 1 produces raw intersection loops on the untrimmed surfaces. Stage 2 splits these loops at the trimming boundaries (Fig. 17c,d). Containment queries then discard invalid segments (shown in red), yielding the final valid intersection curves. We also present a case with trimming curves wrapping in both parametric directions in Figure 18.

5.4.3 Tessellation of Trimmed Surfaces. As a practical application, we use the proposed algorithm to perform tessellation of trimmed periodic surfaces. Efficient rendering of trimmed surfaces requires a tessellation stage. A common approach is to discretize *p*-curves, sample a uniform grid in the parametric domain, and then apply a triangulation strategy such as constrained Delaunay triangulation (CDT). However, triangles lying outside the trimmed region

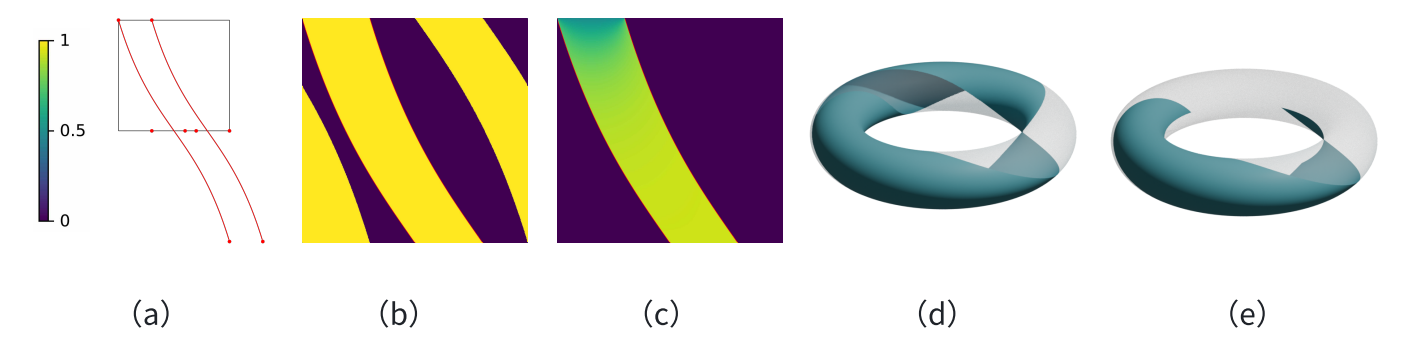


Fig. 16. Comparison between our method and direct winding-number computation on a bi-periodic domain trimmed by double-separation curves. (a) Parameter domain and p-curve loop. (b) Winding number computed in the universal covering space. (c) Winding number computed in the original parameter domain. (d) Containment query result using the proposed method-showing complete trimmed region. (e) Result of direct computation in the physical domains, where part of the region is missing.

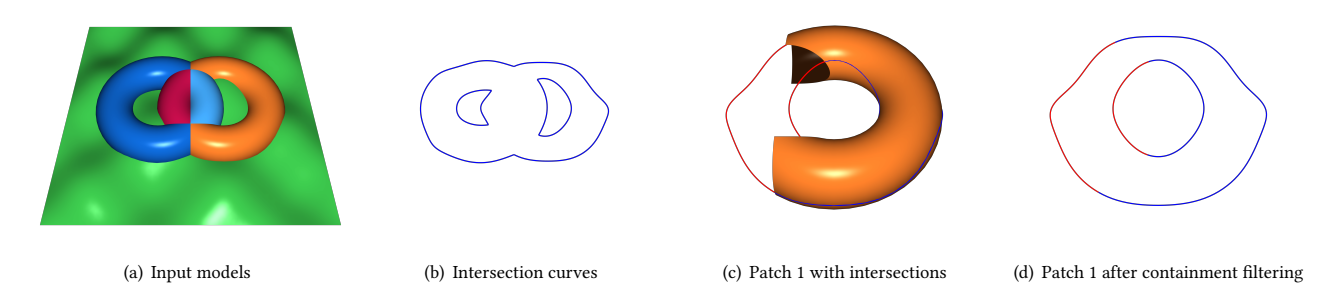


Fig. 17. Intersection between an eight-shaped genus-2 surface and a wave surface. (a) Input models. (b) Intersection curves. (c,d) Raw intersection curves restricted to one surface patch; red segments are removed by containment queries.

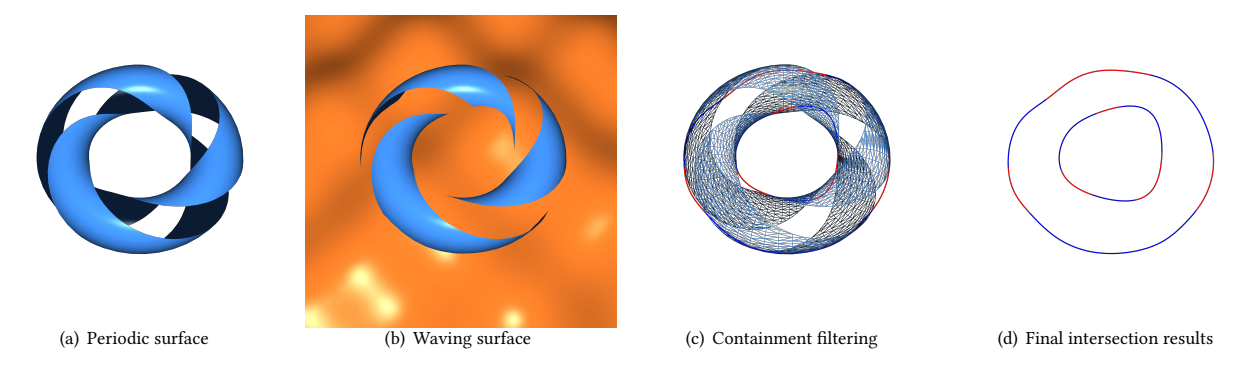


Fig. 18. Intersection between a bi-periodic surface with homology coefficients (p,q) = (2,3) and a waving surface. (a) Input periodic surface. (b) Relative position with respect to the waving surface. (c,d) Containment queries on the periodic surface correctly remove intersections outside the trimmed region.

must subsequently be removed—a step that is often error-prone due to geometric inconsistencies such as open or non-manifold boundaries. Periodic domains present additional challenges, as naïve inside/outside checks fail across periodic boundaries.

With our algorithm, tessellation becomes both efficient and robust, even in the presence of disconnected or imperfect boundaries. Figure 22 shows an example of a surface trimmed by open and nonmanifold boundary curves. Figure 23 demonstrates robust tessellation on a torus-like periodic surface: despite disconnected *p*-curves, our method successfully produces a consistent triangulation of the trimmed region.

6 LIMITATIONS AND FUTURE WORK

Curve Representation. In this paper, we demonstrated an efficient method to compute the winding number given a point and a parametric curve. The parametric curve is represented by the Bézier curve or rational Bézier curve. If the p-curves are given in other forms, a conversion is required, which needs some overhead. For general B-spline curves or even NURBS curves, the upper bound of derivatives can also be efficiently evaluated, but the linear evaluation method still needs to be developed in future work.

Differentiable Trimming. Recently, inverse/differentiable rendering has evolved rapidly. The method for mesh, voxel, and point cloud has been established. Interestingly, [Worchel and Alexa 2023] developed a method to perform differentiable rendering for parametric surfaces via differentiable triangulation. An important topic is whether we can develop differentiable trimming techniques for parametric surfaces.

7 CONCLUSION

In this paper, we presented a novel method for containment queries on trimmed surfaces. By exploiting the bound of Bézier pieces, we designed an accelerating structure for 2D winding number computation. The simplicity of the proposed ellipse bound enables us to use more efficient methods to evaluate the boundary curves without loss of numerical robustness. For the ubiquitous periodic geometric surfaces, we leverage universal covering space to perform inside/outside classification, and simplification methods are used to avoid the infinite computation of winding numbers. Experiment shows our method is efficient, outperforming the existing ray casting method and the winding number method proposed in recent work [Spainhour et al. 2024]. From the aspect of robustness, our method can tolerate geometric errors, spur edges, and a variety of corner cases in the periodic domains.

REFERENCES

- Dana H Ballard. 1981. Strip trees: A hierarchical representation for curves. Commun. ACM 24, 5 (1981), 310–321.
- Gavin Barill, Neil G Dickson, Ryan Schmidt, David IW Levin, and Alec Jacobson. 2018. Fast winding numbers for soups and clouds. ACM Transactions on Graphics (TOG) 37, 4 (2018), 1–12.
- Robert E Barnhill and Scott N Kersey. 1990. A marching method for parametric surface/surface intersection. Computer aided geometric design 7, 1-4 (1990), 257–280.
- Michael Bartoň and Bert Jüttler. 2007. Computing roots of polynomials by quadratic clipping. Computer Aided Geometric Design 24, 3 (2007), 125–141.
- Benson Farb and Dan Margalit. 2011. A primer on mapping class groups (pms-49). Vol. 41. Princeton university press.
- Gerald Farin. 2001. Curves and surfaces for CAGD: a practical guide. Elsevier.
- Nicole Feng, Mark Gillespie, and Keenan Crane. 2023. Winding Numbers on Discrete Surfaces. ACM Trans. Graph (2023).
- Michael S Floater. 1992. Derivatives of rational Bézier curves. Computer Aided Geometric Design 9, 3 (1992), 161–174.
- Simon Flöry and Michael Hofer. 2008. Constrained curve fitting on manifolds. Computer-Aided Design 40, 1 (2008), 25–34.
- Jeffrey Goldsmith and John Salmon. 1987. Automatic creation of object hierarchies for ray tracing. IEEE Computer Graphics and Applications 7, 5 (1987), 14–20.
- Oliver Günther and Eugene Wong. 1990. The arc tree: an approximation scheme to represent arbitrary curved shapes. *Computer Vision, Graphics, and Image Processing* 51, 3 (1990), 313–337.
- Gary Herron. 1985. Smooth closed surfaces with discrete triangular interpolants. Computer Aided Geometric Design 2, 4 (1985), 297–306.
- Michael Hofer and Helmut Pottmann. 2004. Energy-minimizing splines in manifolds. In ACM SIGGRAPH 2004 Papers. 284–293.
- Yixin Hu, Teseo Schneider, Xifeng Gao, Qingnan Zhou, Alec Jacobson, Denis Zorin, and Daniele Panozzo. 2019. TriWild: robust triangulation with curve constraints.

- ACM Transactions on Graphics (TOG) 38, 4 (2019), 1-15.
- Alec Jacobson, Ladislav Kavan, and Olga Sorkine-Hornung. 2013. Robust inside-outside segmentation using generalized winding numbers. ACM Transactions on Graphics (TOG) 32, 4 (2013), 1–12.
- Ligang Liu, Lei Zhang, Binbin Lin, and Guojin Wang. 2009. Fast approach for computing roots of polynomials using cubic clipping. Computer Aided Geometric Design 26, 5 (2009), 547–559.
- Shibo Liu, Ligang Liu, and Xiao-Ming Fu. 2025. Closed-form Generalized Winding Numbers of Rational Parametric Curves for Robust Containment Queries. ACM Transactions on Graphics (TOG) 44, 4 (2025), 1–9.
- Jinesh Machchhar and Gershon Elber. 2016. Revisiting the problem of zeros of univariate scalar Béziers. Computer Aided Geometric Design 43 (2016), 16–26.
- Manish Mandad and Marcel Campen. 2020. Bézier guarding: precise higher-order meshing of curved 2D domains. ACM Transactions on Graphics (TOG) 39, 4 (2020), 103–1
- C. Martens and M. Bessmeltsev. 2025. One-Shot Method for Computing Generalized Winding Numbers. Computer Graphics Forum 44, 5 (2025), e70194. https://doi.org/ 10.1111/cgf.70194 arXiv:https://onlinelibrary.wiley.com/doi/pdf/10.1111/cgf.70194
- Benjamin Marussig and Thomas JR Hughes. 2018. A review of trimming in isogeometric analysis: challenges, data exchange and simulation aspects. Archives of computational methods in engineering 25 (2018), 1059–1127.
- James R Munkres. 2018. Elements of algebraic topology. CRC press.
- Tomoyuki Nishita, Thomas W Sederberg, and Masanori Kakimoto. 1990. Ray tracing trimmed rational surface patches. In *Proceedings of the 17th annual conference on Computer graphics and interactive techniques*. 337–345.
- Steven G Parker, James Bigler, Andreas Dietrich, Heiko Friedrich, Jared Hoberock, David Luebke, David McAllister, Morgan McGuire, Keith Morley, Austin Robison, et al. 2010. Optix: a general purpose ray tracing engine. Acm transactions on graphics (tog) 29, 4 (2010), 1–13.
- Michael J Pratt et al. 2001. Introduction to ISO 10303—the STEP standard for product data exchange. Journal of Computing and Information Science in Engineering 1, 1 (2001), 102–103.
- Gábor Renner and Volker Weiss. 2004. Exact and approximate computation of B-spline curves on surfaces. Computer-Aided Design 36, 4 (2004) 351–362
- curves on surfaces. Computer-Aided Design 36, 4 (2004), 351–362. Steven M Rubin and Turner Whitted. 1980. A 3-dimensional representation for fast rendering of complex scenes. In Proceedings of the 7th annual conference on Computer graphics and interactive techniques. 110–116.
- Takis Sakkalis, Rida T Farouki, and Leonid Vaserstein. 2009. Non-existence of rational arc length parameterizations for curves in Rn. J. Comput. Appl. Math. 228, 1 (2009), 494–497.
- Andre Schollmeyer and Bernd Froehlich. 2018. Efficient and anti-aliased trimming for rendering large NURBS models. IEEE Transactions on Visualization and Computer Graphics 25, 3 (2018), 1489–1498.
- Andre Schollmeyer and Bernd Fröhlich. 2009. Direct trimming of NURBS surfaces on the GPU. ACM Transactions on Graphics (TOG) 28, 3 (2009), 1–9.
- Jaroslav Sloup and Vlastimil Havran. 2021. Optimizing Ray Tracing of Trimmed NURBS Surfaces on the GPU. In Computer Graphics Forum, Vol. 40. Wiley Online Library, 161–172.
- Jacob Spainhour, David Gunderman, and Kenneth Weiss. 2024. Robust Containment Queries over Collections of Rational Parametric Curves via Generalized Winding Numbers.
- Jacob Spainhour and Kenneth Weiss. 2025. Robust Containment Queries over Collections of Trimmed NURBS Surfaces via Generalized Winding Numbers. arXiv preprint arXiv:2504.11435 (2025).
- Haoran Sun, Jingkai Wang, Hujun Bao, and Jin Huang. 2024. GauWN: Gaussian-smoothed Winding Number and its Derivatives. In SIGGRAPH Asia 2024 Conference Papers. 1–9
- Markus Worchel and Marc Alexa. 2023. Differentiable Rendering of Parametric Geometry. ACM Transactions on Graphics (TOG) 42, 6 (2023), 1–18.
- Paweł Woźny and Filip Chudy. 2020. Linear-time geometric algorithm for evaluating Bézier curves. *Computer-Aided Design* 118 (2020), 102760.
- Paweł Woźny and Filip Chudy. 2025. Fast subdivision of Bézier curves. arXiv preprint arXiv:2509.15691 (2025).

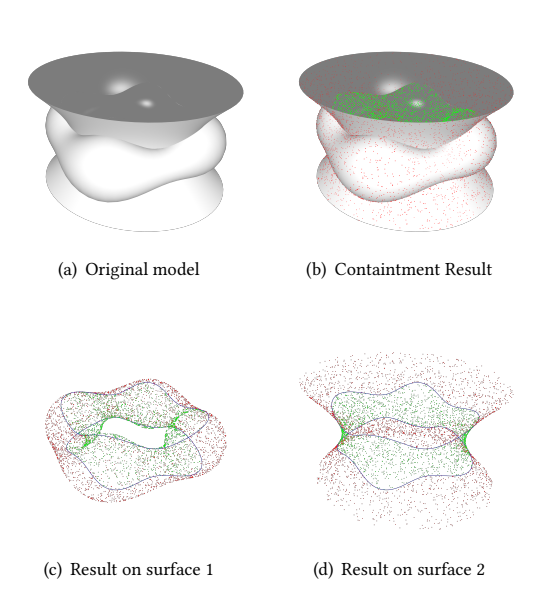


Fig. 19. Containtment queries on a B-Rep model with multiple patches. The surface is generated by union between a hyperbolid surface and defromed torus. Blue curves are intersection curves between two surface. Samples were generated on the geometric surfaces.

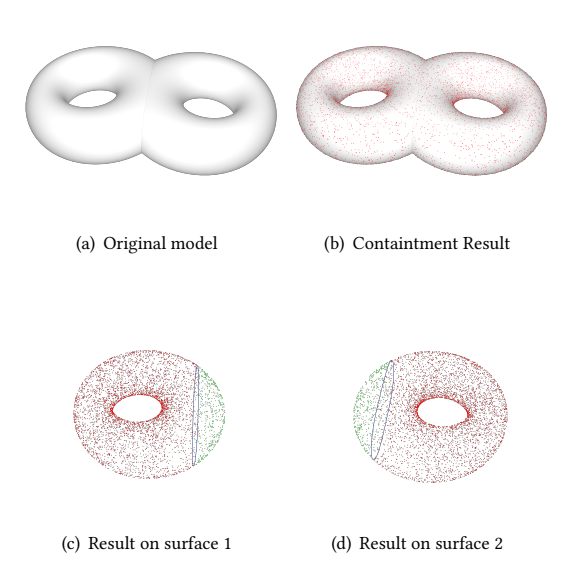


Fig. 20. Containtment queries on a genus 2 B-Rep model defined by the union of two torus like surfaces. Blue curves are intersection curves between two surface. Samples were generated on the geometric surfaces.

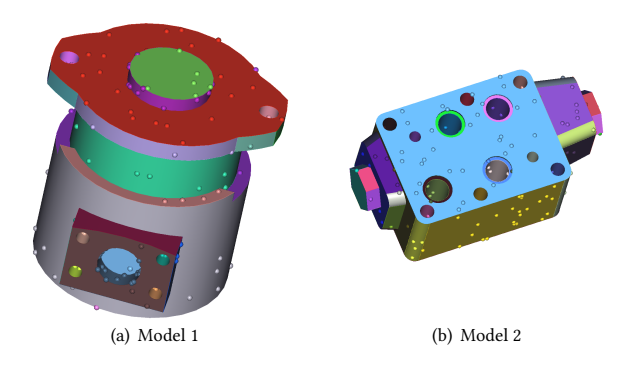


Fig. 21. Real world models. We randomly generate some points on the underlying geometric surfaces and use proposed algorithm to select the points on the boundary of B-Rep model.

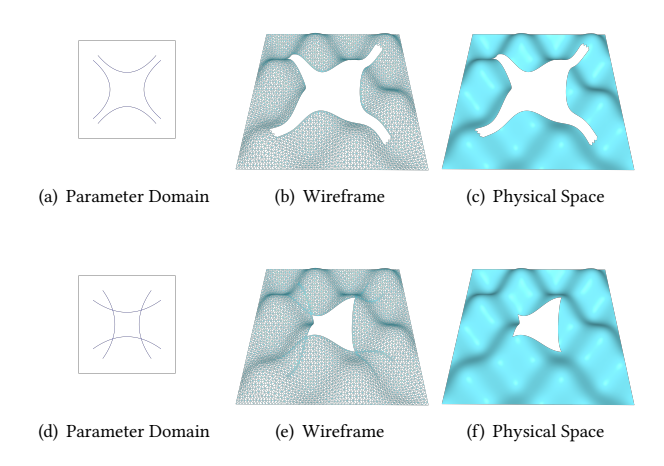


Fig. 22. Illustration of robust periodic trimmed surface tessellation. First row: tessellation of surface with open boundary curves. Second row: tessellation of surface with non-manifold boundary curves.

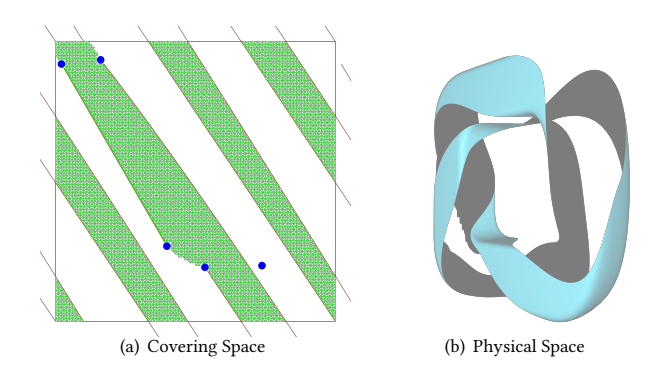


Fig. 23. Illustration of robust periodic trimmed surface tessellation. The black rectangle is boundary of parameter domain. Blue points are control points of the boundary curves. Even the boundary curves are not end-to-end continuous, our method can generate reasonable tessellation result.

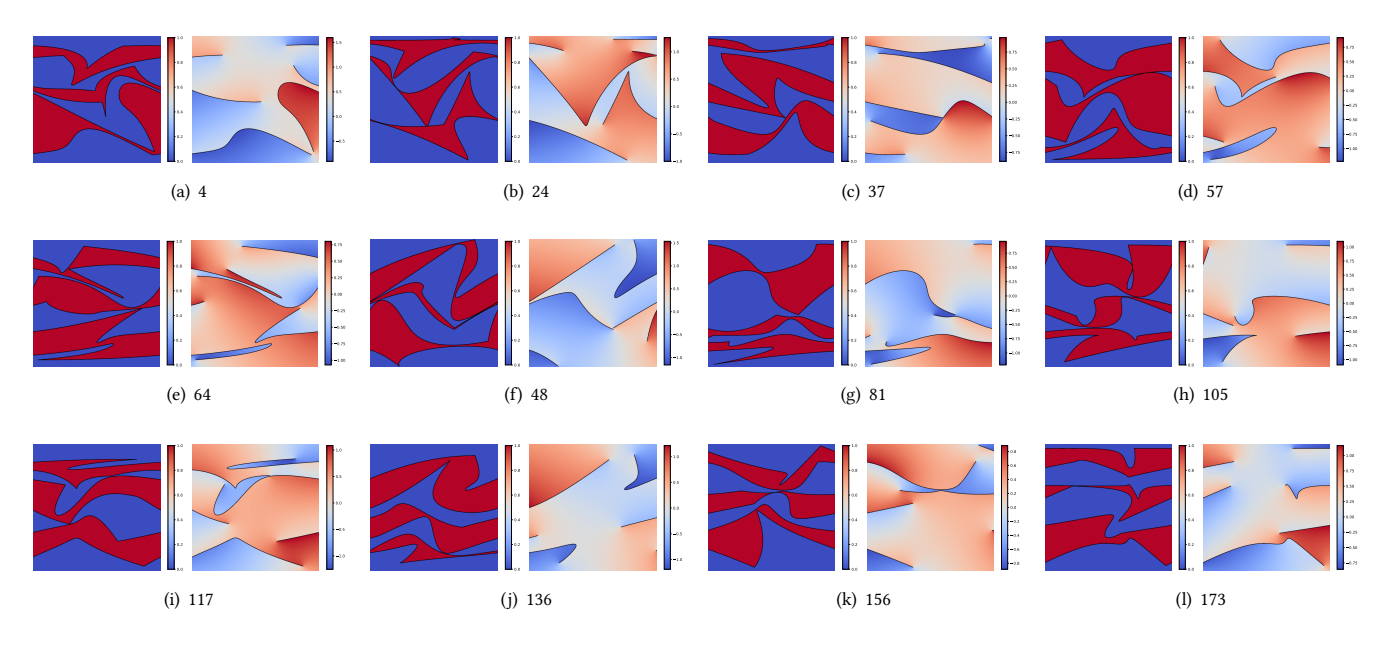


Fig. 24. Samples from the periodic dataset A. For each subfigure, the left part is the winding number computed by the periodic method in covering space and the right is the simply computed winding number in parametric domain.

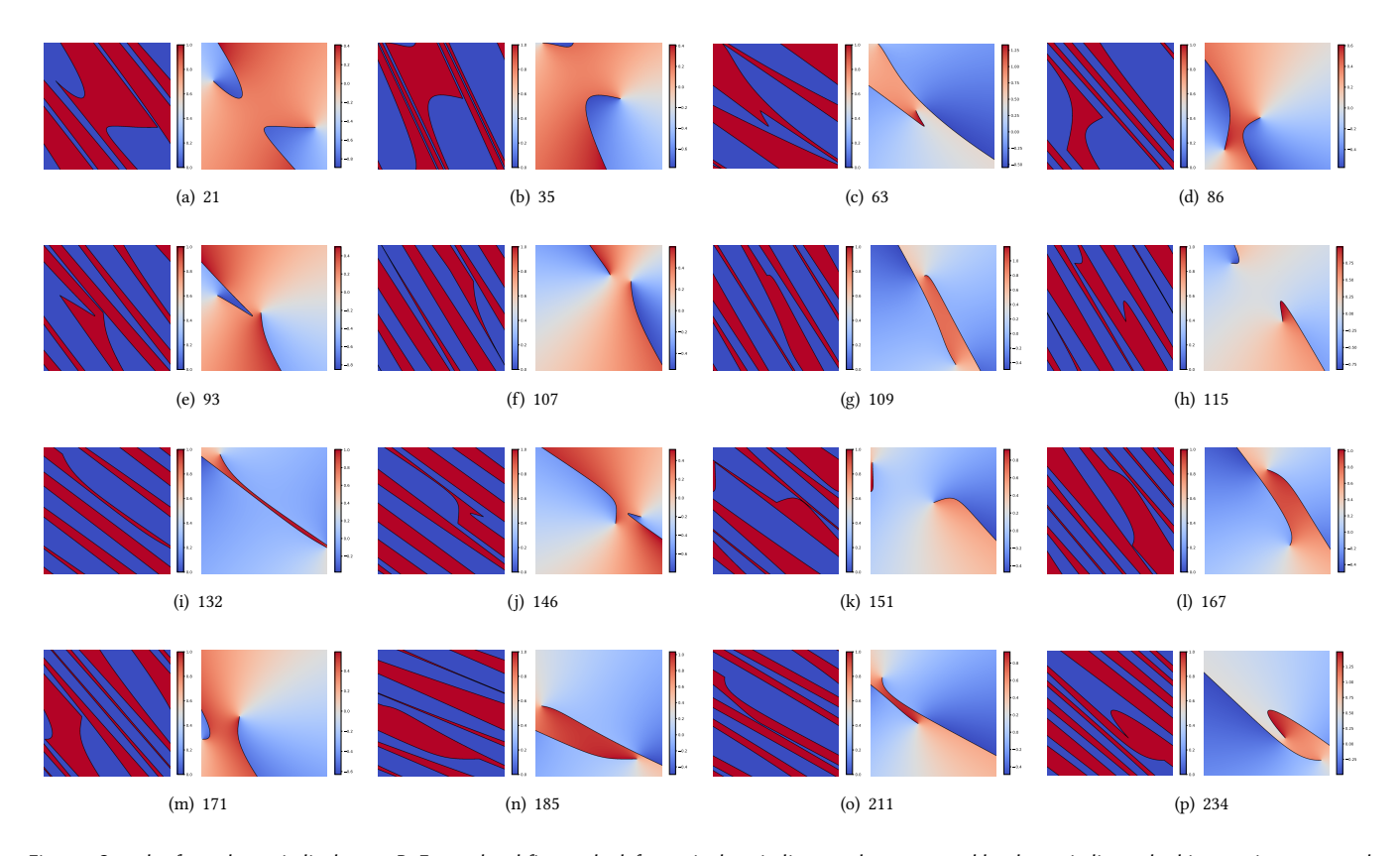


Fig. 25. Samples from the periodic dataset B. For each subfigure, the left part is the winding number computed by the periodic method in covering space and the right is the simply computed winding number in parametric domain.

PROOFS OF THE ELLIPSE BOUND

Boundedness and the Rational Case

In this section, we present the detailed derivation of the ellipse bound. Firstly, we prove the lemma 4.1

PROOF. Let $p = \gamma(t)$ for some $t \in [0, 1]$. Suppose, for contradiction, that $p \notin \Omega_{\gamma}$. Then

$$d(p, \gamma(0)) + d(p, \gamma(1)) > B.$$
 (14)

However, since the curve length between $\gamma(0)$ and $\gamma(t)$ is $\int_0^t \|\gamma'(u)\| du$ and similarly for $\gamma(t)$ to $\gamma(1)$, we have

$$d(p,\gamma(0)) + d(p,\gamma(1)) \le \int_0^t \|\gamma'(u)\| du + \int_t^1 \|\gamma'(u)\| du \le B, (15)$$

which contradicts the assumption. Hence, $\gamma \subset \Omega_{\gamma}$.

For a polynomial Bézier curve defined by control points $\{P_i\}_{i=0}^n$, an upper bound for its derivative norm can be obtained from its hodograph. The hodograph is itself a Bézier curve with control points ${n(P_i - P_{i-1})}_{i=1}^n$, yielding the bound

$$B = \max_{1 \le i \le n} n ||P_i - P_{i-1}||.$$

For a rational Bézier curve with control points $\{P_i\}_{i=0}^n$ and weights $\{w_i\}_{i=0}^n$, similar derivative bounds are available in the literature. Following Floater [1992], two possible bounds for $\|\gamma'(t)\|$ are:

$$\|\gamma'(t)\| \le n \frac{W}{w} \max_{i,j} \|P_i - P_j\|,$$
 (16)

$$\|\gamma'(t)\| \le n \frac{W^2}{w^2} \max_i \|P_i - P_{i-1}\|,$$
 (17)

where $W = \max_i w_i$ and $w = \min_i w_i$.

A.2 **Termination**

In this subsection, we proof the Lemma 4.2. The key insight is that each subdivision halves the diameter of the bounding ellipse.

PROOF. Let the recursion depth be m. At this level, the diameter of the bounding ellipse is $B/2^m$.

- If $d > \epsilon$ and $m \ge \log(B/\epsilon)$, the test point p cannot lie within any ellipse at this depth, and the recursion terminates.
- If $d \le \epsilon$, let q be the closest point on y to p. There exists an endpoint v of the current subsegment such that

$$||v-q||<\frac{B}{2^m}.$$

Thus,

$$||p - v|| \le ||p - q|| + ||q - v|| < d + \frac{B}{2^m}.$$

When $m \ge \log(B/\epsilon) + 1$, we have $\frac{B}{2^m} < \epsilon/2$, so

$$||p-v|| < d + \frac{\epsilon}{2}.$$

- If $d \le \epsilon/2$, then $||p v|| < \epsilon$, and the algorithm reports "boundary".
- If $d > \epsilon/2$, the ellipse diameter is already smaller than $\epsilon/2$, meaning the test point lies outside all bounding ellipses, and recursion terminates.

PROOFS OF THE PERIODIC CASE

Throughout, a *simple loop* refers to a loop without self-intersections.

B.1 Proof of Proposition 4.3

Proposition B.1. Let S be a surface homeomorphic to a cylinder, and let y be a simple loop on S. Then the homology coefficient n of y satisfies $n \in \{0, \pm 1\}$.

PROOF. Let p denote the projection map from the cylinder to S^1 . If $|n| \ge 2$, then the composed mapping $p \circ \gamma : S^1 \to S^1$ is non-injective. Hence, there exist $t_1, t_2 \in S^1$ such that $p \circ \gamma(t_1) = p \circ \gamma(t_2)$, implying that $\gamma(t_1)$ and $\gamma(t_2)$ lie on the same vertical line. This results in a self-intersection of γ , contradicting its simplicity.

Proposition B.2. Let S be a surface homeomorphic to a torus, and let y be a simple loop on S with homology coefficients (n, m). If n = 0, then $m \in \{0, \pm 1\}$; similarly, if m = 0, then $n \in \{0, \pm 1\}$.

PROOF. We prove only the case n = 0 and $m \ge 2$; the other cases are symmetric. Lift y to the universal covering space, obtaining a simple curve $\tilde{\gamma}$. Let H be the subgroup of deck transformations generated by (0, 1); then the quotient $C = \mathbb{R}^2/H$ is homeomorphic to an infinite cylinder. Denote the quotient map by q. The image $q(\tilde{\gamma})$ is a loop with homology coefficient m. By Proposition B.1, since $m \ge 2$, $q(\tilde{\gamma})$ must self-intersect, implying that γ is not simple.

We now recall two classical results from topology [Farb and Margalit 2011] concerning simple loops and their intersection properties.

Proposition B.3. Let S be a surface homeomorphic to a torus, and let α and β be generators of $H_1(S,\mathbb{Z})$. If a simple loop γ on S satisfies $\gamma = n\alpha + m\beta$, then m and n are coprime.

PROPOSITION B.4. Let S be a surface homeomorphic to a torus. If γ_1 and γ_2 are two loops on S with homology coefficients (n_1, m_1) and (n_2, m_2) , respectively, then the minimal intersection number between them is

$$i((n_1, m_1), (n_2, m_2)) = |n_1 m_2 - n_2 m_1|.$$
 (18)

From Proposition B.4, we obtain the following corollary.

Proposition B.5. Let S be a surface homeomorphic to a torus, and let $\{\gamma_i\}$ be a collection of disjoint simple loops on S with homology coefficients (n_i, m_i) . Then each loop satisfies either $(n_i, m_i) = (0, 0)$ or $(n_i, m_i) = \pm (a, b)$ for some fixed integers a, b.

PROOF. If either $n_i = 0$ or $m_i = 0$, Propositions B.1 and B.2 yield the result. Now suppose that all coefficients are nonzero.

By Proposition B.4, if γ_i and γ_j are disjoint, then $n_i m_j - n_j m_i = 0$. Since all terms are nonzero, this implies $n_i/m_i = n_i/m_i$. Because n_i and m_i are coprime (Proposition B.3), we conclude that $(n_i, m_i) =$ $\pm(n_j,m_j).$

Finally, Proposition B.5 allows us to classify all loops, completing the proof of Proposition 4.3.

B.2 Proof of Proposition 4.4

Proposition 4.4 can be understood as a partitioning of all lifted curves into disjoint periodic families. A concise proof is as follows.

PROOF. Let $c_{i,j} = \gamma + i\vec{c}_1 + j\vec{e}_2$. For all integers i, j, each $c_{i,j}$ is contained in the right-hand side of the equation. Write i = ap + b with $a \in \mathbb{Z}$ and $0 \le b < p$. Then

$$c_{i,j} = c_{b,j-aq} + ap\vec{e}_1 + aq\vec{e}_2 \subset \gamma_{b,j-aq}.$$

Hence, the left-hand side is contained in the right-hand side. Conversely, it is straightforward to verify that the right-hand side is contained in the left-hand side, completing the proof.

C IMPLEMENTATION DETAILS

In this section, we provide pesudo code of proposed algorithms and introduce some tedious details of our algorithm. We also refer readers to our C++ implementation (Anonymous).

C.1 Periodic Winding Number Computation

In this section, we list the pesudo code of winding number computation method.

In our implementation, to avoid translating parametric curves, we use the following property of winding number: Let \vec{v} be a two dimensional vector, p is the test point and γ is a curve, then we have

$$\omega(p, \gamma + \vec{v}) = \omega(p - \vec{v}, \gamma) \tag{19}$$

For uni-periodic case, algorithm 2 shows the pesudo code of the method computing winding number with respect to a periodically extended curve (section 4.4) and algorithm 3 illustrated the method handling contractible case.

For bi-periodic case, algorithm 4 demonstrates the contractible case and algorithm 6 presents the bi-periodic winding number computation implementation.

C.2 Pairing Curves in Bi-periodic Case

In this section, we describe the algorithm detial of pairing the extended curves properly. Given a set of lift curves, we firstly split them to three set as defined in proposition 4.3. Suppose $A = \{\alpha_i\}_{i=1}^m$ and $B = \{\beta_i\}_{i=1}^m$, the output of pairing algorithm is two curve sets $\{\tilde{\gamma}_i\}$ and $\{\bar{\gamma}_i\}$, such that $\tilde{\gamma}_i = \alpha_{l,(r,s)}$ and $\bar{\gamma}_i = \beta_{l_i,(r,s)} + \vec{v}_i$ is a proper pair. The term *proper* means that $\bar{\gamma}_{l,(r,s)}$ is the first periodically extended curve on the left of $\tilde{\gamma}_i$.

If we directly set $\bar{\gamma}_i = \beta_i$, the band defined by periodically extended loop pairs may overlap, as illustrated in Figure 26. We can solve this issue by proper pairing strategy.

Firstly, we define a *ToLeft* predicate (see algorithm 7) between curves $\gamma_{k,(i,j)}$. We say that $\gamma_{k',(i',j')}$ is on the left of $\gamma_{k,(i,j)}$ if for some point $p \in \gamma_{k',(i',j')}$, the winding number $\omega(p,\gamma_{k,(i,j)})$ is positive. In our setup, the ToLeft predicate defines a partial order in set $\{\gamma_{k,(i,j)}\}_{i,j\in\mathbb{Z}}$ since these curves are insersection-free and periodically extended with same extenison per period.

With this predicate, finding $\bar{\gamma}_k$ likes the process of finding "smallest number". Algorithm 8 shows an algorithm find the smallest $\beta_{(i,j)}$ on the left of $\alpha_{(0,0)}$ and Algorithm 9 generate the pairs $\tilde{\gamma}_i$ and $\bar{\gamma}_i$ properly.

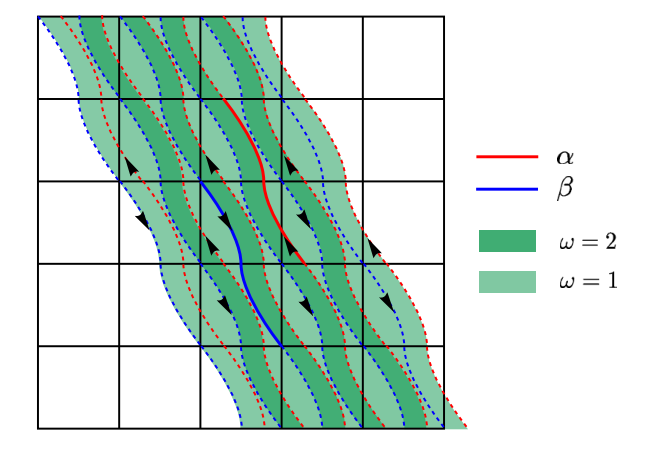


Fig. 26. If the original lifted curve α and β are in improper place, directly use pairing will lead to overlap between regions defined by $\alpha_{r,s}$ and $\beta_{r,s}$. The original lift of α and β are represented by solid curves and other copies are illustrated by dashed curves. Winding number field ω defined by curves are plotted, overlapped regions have $\omega=2$.

Algorithm 2 PeriodicExtendedWindingNumber

Return ω

```
Require: 2D path \gamma, test point p, tolerance value \epsilon.
Ensure: Winding number of the pre-images of y w.r.t. p.
   l \leftarrow LeftMostContorlPoint(y).x
   r \leftarrow RightMostControlPoint(\gamma).x
                                                           ▶ Use y coordinates if
   |l - r| = 0. Here we omit those y-code.
   \vec{v} \leftarrow \gamma(1) - \gamma(0)
   for k > 0 do
        p' = p - k\vec{v}
        if p.x - k < l then
            break
       \omega \leftarrow \omega + WindingNumber(p', \gamma, \epsilon)
        \omega \leftarrow \omega - WindingNumberLineSegment(p', \gamma(0), \gamma(1))
   end for
   for k > 0 do
        p' \leftarrow p + k\vec{v}
       if p.x + k > r then
            break
        end if
        \omega \leftarrow \omega + WindingNumber(p', \gamma, \epsilon)
        \omega \leftarrow \omega - WindingNumberLineSegment(p', \gamma(0), \gamma(1))
   \omega \leftarrow \omega + WindingNumberLine(p', \gamma(0), \gamma(1))
```

Algorithm 3 UniperiodicContractibleWindingNumber

```
Require: 2D closed loop \gamma, test point p, tolerance value \epsilon.
Ensure: Winding number of the pre-images of y w.r.t. p.
  l \leftarrow LeftMostContorlPoint(\gamma).x
  r \leftarrow RightMostControlPoint(\gamma).x
                                                       \triangleright Use y coordinates if
  |l - r| = 0. Here we omit those y-code.
  for k > 0 do
       p' = p - k\vec{v}
       if p.x - k < l then
            break
       end if
       \omega \leftarrow \omega + WindingNumber(p', \gamma, \epsilon)
   end for
  for k > 0 do
       p' \leftarrow p + k\vec{v}
       if p.x + k > r then
            break
       end if
       \omega \leftarrow \omega + WindingNumber(p', \gamma, \epsilon)
   end for
   Return \omega
```

Algorithm 4 BiperiodicContractibleWindingNumber

```
Require: 2D closed loop \gamma, test point p, tolerance value \epsilon.
Ensure: Winding number of the pre-images of \gamma w.r.t. p.
   l \leftarrow LeftMostContorlPoint(\gamma).x
   r \leftarrow RightMostControlPoint(\gamma).x
   t \leftarrow TopMostControlPoint(\gamma).y
   b \leftarrow BottomMostControlPoint(\gamma).y
   h \leftarrow \lceil t - b \rceil, v \leftarrow \lceil r - l \rceil
   \omega \leftarrow 0
   for i in [-h, h] do
        for j in [-v, v] do
             p' \leftarrow p - (i, j)
             \omega \leftarrow \omega + WindingNumber(p', \gamma)
        end for
   end for
   Return \omega
```

Algorithm 5 PeriodicPairWN

```
Require: 2D path \gamma_1, \gamma_2, test point p, tolerance value \epsilon.
Ensure: Winding number of the pre-images of y w.r.t. p.
  \omega_1 \leftarrow PeriodicExtendedWindingNumber(p, \gamma_1, \epsilon)
  \omega_2 \leftarrow PeriodicExtendedWindingNumber(p, \gamma_2, \epsilon)
   Return \omega_1 + \omega_2
```

Algorithm 6 ComputeBiperiodicWindingNumber

```
Require: test point p, tolerance value \epsilon.
Ensure: Winding number of the pre-images of y w.r.t. p.
   for All pairs \tilde{\gamma}_k, \bar{\gamma}_k do
        for i in [0, n) do
            for j in [-|m|, |m|] do
                  \omega \leftarrow \omega + PeriodicPairWN(p - (i, j), \tilde{\gamma}_k, \bar{\gamma}_k)
             end for
        end for
   end for
   Return \omega
```

Algorithm 7 ToLeft

```
Require: 2D path \gamma_1, \gamma_2.
Ensure: true if \gamma_1 is on the left of \gamma_2, otherwise false.
   \omega = PeriodicExtendedWindingNumber(\gamma_1(0.5), \gamma_2)
   Return \omega > 0
```

Algorithm 8 PairLoop

```
Require: 2D path \alpha \in A, \beta \in B.
Ensure: \vec{v} \in \mathbb{R}^2, such that the region defined by the lift curves of \alpha
   and \beta + v containes no other preimages of \alpha or \beta
   p, q \leftarrow homology coefficients of set A
   \vec{v} = q\vec{e}_2
   for i in [0, p) do
        for j in [-q, q] do
             if ToLeft(\beta + (i, j), \alpha) and ToLeft(\beta + (i, j), \beta + \vec{v}) then
                  \vec{v} \leftarrow (i, j)
             end if
        end for
   end for
   Return \vec{v}
```

Received 20 February 2007; revised 12 March 2009; accepted 5 June 2009

```
Algorithm 9 PairLoops
Require: 2D path \gamma_i.
Ensure: Winding number of the pre-images of \gamma w.r.t. p.
   A, B, C \leftarrow SplitLoops(\{\gamma_i\})
   n \leftarrow SizeOf(A)
   for i in [0, n) do
         \tilde{\gamma}_i = \alpha_i = A[i]
         \bar{\gamma}_i = NULL
         toRemove = NULL \\
         for \beta in B do
              \bar{\gamma} \leftarrow PairLoop(\alpha_i, \beta)
              if \bar{\gamma}_i is NULL or ToLeft(\bar{\gamma}, \bar{\gamma}_i) then
                   \bar{\gamma}_i \leftarrow \bar{\gamma}
                   toRemove \leftarrow \bar{\gamma}
              end if
         end for
         Remove \alpha_i from A
         Remove toRemove from B
   end for
   Return \{\tilde{\gamma}_i\} and \{\bar{\gamma}_i\}
```